

NJC

Accepted Manuscript



This article can be cited before page numbers have been issued, to do this please use: K. Takagi, Y. Yamada, R. Fukuda, M. Ehara and D. Takeuchi, *New J. Chem.*, 2018, DOI: 10.1039/C8NJ00455B.



This is an Accepted Manuscript, which has been through the Royal Society of Chemistry peer review process and has been accepted for publication.

Accepted Manuscripts are published online shortly after acceptance, before technical editing, formatting and proof reading. Using this free service, authors can make their results available to the community, in citable form, before we publish the edited article. We will replace this Accepted Manuscript with the edited and formatted Advance Article as soon as it is available.

You can find more information about Accepted Manuscripts in the [author guidelines](#).

Please note that technical editing may introduce minor changes to the text and/or graphics, which may alter content. The journal's standard [Terms & Conditions](#) and the ethical guidelines, outlined in our [author and reviewer resource centre](#), still apply. In no event shall the Royal Society of Chemistry be held responsible for any errors or omissions in this Accepted Manuscript or any consequences arising from the use of any information it contains.



ESIPT Emission Behavior of Methoxy-Substituted 2-Hydroxyphenylbenzimidazole Isomers

Koji Takagi,^{a*} Yoshihiro Yamada,^a Ryoichi Fukuda,^{b,c*} Masahiro Ehara,^{b,c} and Daisuke Takeuchi^d

Received 00th January 20xx,
Accepted 00th January 20xx

DOI: 10.1039/x0xx00000x

www.rsc.org/

Three 2-hydroxyphenylbenzimidazole isomers **1**, **2**, and **3** having the methoxy group at the 6, 4, and 3-position, respectively, were synthesized in short steps. **1** exhibited the ESIPT emission irrespective of the solvent character. While **2** only showed the ESIPT emission in THF and MeCN, the LE emission was also observed in MeOH and THF/water mixed solvent. These phenomena were nicely accounted for by the intramolecular hydrogen bonding interaction. The fluorescence spectra of **3** always consisted of two emission bands and exhibited strange behaviors particularly in protic solvents. The fluorescence emissions in the solid state were found to be closely related to the crystal packing structure.

Introduction

Fluorescent molecules can be potentially applied to organic light-emitting diodes, lasers, chemosensors, bioimaging, and so on.^{1–3} The excited-state intramolecular proton transfer (ESIPT) have been attracting considerable interest because of the large Stokes shift that is the energy difference between the absorption and emission peak maxima. The large Stokes shift can prevent the fluorescence self-quenching. Therefore fluorescent molecules capable of ESIPT are desirable optoelectronic materials as a result of the bright light emission even in the solid state.^{4,5} ESIPT-active molecules normally adopt the enol (E) form in the ground state, while the keto (K*) form is generated upon the photo-excitation although this is not always the case. The formation of an intramolecular hydrogen bonding often facilitates the so-called four-level cyclic proton-transfer process (E–E*–K*–K–E).^{6,7} Many ESIPT-active oxazole, thiazole, and imidazole compounds carrying the 2-hydroxyphenyl group have been attracting great interest. In particular, a diverse set of imidazole derivatives were designed and synthesized. Park et al have reported many ESIPT-active compounds based on the 2-(2'-hydroxyphenyl)imidazole unit for the material application.^{8–12} Mutai et al have prepared structurally-relevant 2-(2'-hydroxyphenyl)imidazo[1,2-a]pyridine derivatives to reveal the color-tunability by the

substituent effect^{13,14} and polymorph-dependent luminescence.^{15,16} Gryko et al have synthesized π -extended ESIPT-active imidazole derivatives^{17,18} to investigate the structure-property relationship in detail.

The formation of an intramolecular hydrogen bonding is preferable for providing ESIPT, however, this is not a sufficient condition for the efficient ESIPT emission. As Park et al¹⁹ and Tsai et al²⁰ have pointed out, the transition to the excited-state twisted intramolecular charge transfer (S_1 -T_{ICT}) states is responsible for the non-radiative decay from the excited state and low fluorescence quantum yield. In order to realize the efficient ESIPT emission, compounds having the restricted conformation with the proton donor and acceptor units in the proximal position have been synthesized.^{21–24}

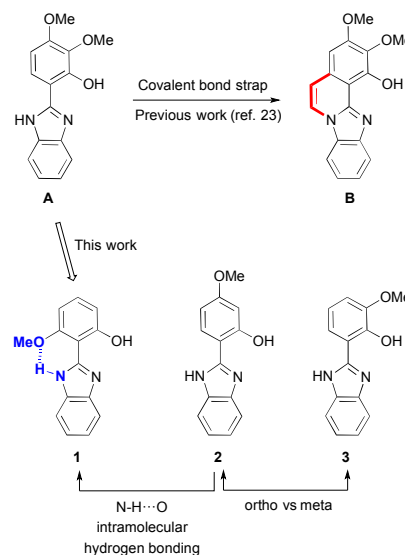


Fig. 1 2-Hydroxyphenylbenzimidazole derivatives for efficient ESIPT and reference compounds.

^a Graduate School of Engineering, Nagoya Institute of Technology, Gokiso-cho, Showa-ku, Nagoya 466-8555.

^b Research Center for Computational Science and Institute for Molecular Science, 38 Nishigo-naka, Myodaiji, Okazaki 444-8585.

^c Elements Strategy Initiative for Catalysts and Batteries, Kyoto University, 1-30 Goryo-Ohara, Nishikyo-ku, Kyoto 615-8245.

^d Laboratory of Chemistry and Life Science Institute of Innovative Research, Tokyo Institute of Technology, Nagatsuta-cho 4259, Midori-ku, Yokohama 226-8503.
E-mail: takagi.koji@nitech.ac.jp

Electronic Supplementary Information (ESI) available: NMR spectra, optical properties, and computational results. CCDC 1815097, 1815098, and 1815099. See DOI: 10.1039/x0xx00000x

In line with these successful examples, we have prepared a fluorescent imidazole compound **B** (Fig. 1) to figure out that the structure rigidification is a promising way to realize the efficient ESIPT emission.^{25–27} The product was obtained by the acid-catalyzed intramolecular cyclization of a precursor bearing the acetal-protected aldehyde group. Although ESIPT could be enhanced as compared with a non-fused compound **A**, the synthetic route required five steps starting from a commercially available compound. Herein, we have succeeded in realizing the efficient ESIPT emission by means of an intramolecular hydrogen bonding between amine and ether oxygen instead of the covalent bond strap (Fig. 1, compound **1**). To clearly demonstrate the efficacy of N-H...O intramolecular hydrogen bonding in **1**, the fluorescent properties of compounds **2** and **3** were also studied. Both **1** and **2** have the methoxy group at the meta-position relative to the hydroxy group, but only **1** can form N-H...O intramolecular hydrogen bonding. The comparison of **2** with **3** was intended to reveal the resonance effect of the methoxy group on the fluorescence emission. It is to be noted that all compounds can be prepared in short steps from commercially available compounds.

Experimental

Instruments

¹H- and ¹³C-nuclear magnetic resonance (NMR) spectroscopies were obtained on a Bruker Avance III HD NanoBay 400 FT-NMR spectrometers using tetramethylsilane (¹H-NMR) and solvent residual peaks (¹³C-NMR) as the internal standard. Melting points (Mp) were determined on a Yanaco micro melting point apparatus MP-500D. Elemental analyses (EA) were performed on a Elementar vario EL cube in the CHN mode. Ultraviolet-visible (UV-vis) and fluorescence spectra in solutions were recorded on a Shimadzu UV-1650 spectrophotometer and a Shimadzu RF-5300 spectrofluorometer, respectively, using a 10 mm quartz cell. Fluorescence quantum yields (QYs) were determined relative to quinine sulfate in 0.1 M H₂SO₄ having a QY of 0.55. Fluorescence spectra in powders were recorded on a Hamamatsu Quantaurus-QY Plus C13534 instrument and absolute QYs were obtained with an integrating sphere C11347. The crystallographic data were collected on a Bruker SMART APEX II ULTRA/CCD diffractometer equipped with monochromated Mo K α radiation ($\lambda = 0.71073 \text{ \AA}$) at 90 K. Calculations were carried out using the program packages APEX III and ShelXle for Windows. The positional and thermal parameters of non-hydrogen atoms were refined anisotropically on F^2 by the full-matrix least-squares method using SHELXL-2014. Hydrogen atoms were placed at calculated positions and refined with a riding mode on their corresponding carbon atoms. Theoretical calculations were performed using Gaussian 09 (Revision E.01) package of programs. The ground and excited state structures were optimized with DFT/TDDFT calculations at the PBE0/aug-cc-pVDZ (for C, N, O)/cc-pVDZ (for H) level of theory, and the vertical transition energies and oscillator strengths were calculated. Solvent effect was considered by the IEF PCM

(integral equation formula polarizable continuum model). For electronic excitation from the ground state (absorption spectrum), the linear response formalism was used, while for emission from the first excited state (fluorescence spectrum), the state-specific external-iteration method and non-equilibrium solvation formalism were used.

Materials

All materials were obtained from commercial suppliers and used as received. 2-Hydroxy-6-methoxybenzaldehyde²⁸ and 2-(2'-hydroxy-3'-methoxyphenyl)-1H-benzimidazole (**3**)²⁹ were prepared as reported previously.

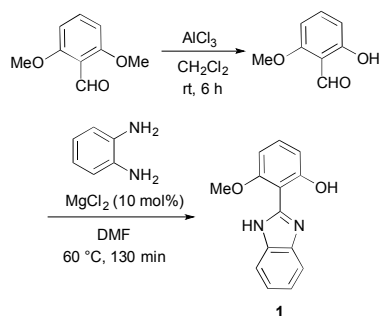
2-(2'-Hydroxy-6'-methoxyphenyl)-1H-benzimidazole (1). To a flask containing 2-hydroxy-6-methoxybenzaldehyde (1.51 g, 9.93 mmol) and *o*-phenylenediamine (1.07 g, 9.93 mmol) were added DMF (50 mL) and MgCl₂ (95.5 mg, 0.993 mmol), and the mixture was heated at 60 °C for 130 min under oxygen atmosphere. After removing DMF in vacuo, ethyl acetate and water were added. An aqueous phase was extracted with ethyl acetate, and the combined organic phase was rinsed with brine and dried over Na₂SO₄. After evaporating solvents, the obtained crude product was washed with methanol to give analytically pure yellow solid (785 mg, 33% yield). Mp. 213.8–217.2 °C. ¹H-NMR (DMSO-*d*₆, ppm) 4.06 (s, 3H), 6.69 (d, *J*=8.31 Hz, 1H), 6.66 (d, *J*=8.31 Hz, 1H), 7.17–7.46 (3H), 7.71 (d, *J*=9.05 Hz, 2H), 12.3 (s, 1H), 14.5 (s, 1H). ¹³C-NMR (DMSO-*d*₆, ppm) 56.5, 102.0, 102.1, 110.5, 112.7, 117.8, 122.9, 123.4, 132.2, 133.0, 139.5, 150.4, 158.3, 160.7. Anal. Calcd. for C₁₄H₁₂N₂O₂: C, 69.99%; H, 5.03%; N, 11.66%. Found: C, 69.58%; H, 5.24%; N, 11.41%.

2-(2'-Hydroxy-4'-methoxyphenyl)-1H-benzimidazole (2). This compound was synthesized in a similar manner to that of **1**. The crude product was washed with THF and recrystallized from ethanol to give yellow solid (6% yield). Mp. 224.6–226.1 °C. ¹H-NMR (DMSO-*d*₆, ppm) 3.82 (s, 3H), 6.56–6.73 (2H), 7.20–7.34 (2H), 7.49–7.79 (2H), 7.96 (d, *J*=8.80 Hz, 1H), 13.0 (s, 1H), 13.4 (s, 1H). ¹³C-NMR (DMSO-*d*₆, ppm) 54.8, 100.9, 105.1, 106.0, 110.6, 117.0, 121.7, 122.2, 126.7, 132.5, 140.2, 151.5, 159.4, 161.7. Anal. Calcd. for C₁₄H₁₂N₂O₂: C, 69.99%; H, 5.03%; N, 11.66%. Found: C, 69.61%; H, 5.21%; N, 11.37%.

Results and discussion

2-(2'-Hydroxy-4'-methoxyphenyl)-1H-benzimidazole (**2**) and 2-(2'-hydroxy-3'-methoxyphenyl)-1H-benzimidazole (**3**) were synthesized in one step from commercially available materials with a catalytic amount of MgCl₂ (10 mol%) in wet DMF under oxygen atmosphere.²⁹ The oxygen atmosphere was preferable for the complete conversion from 2,3-dihydro-1H-benzimidazoles to 1H-benzimidazoles. As for 2-(2'-hydroxy-6'-methoxyphenyl)-1H-benzimidazole (**1**), 2-hydroxy-6-methoxybenzaldehyde was obtained by the selective mono demethylation of 2,6-dimethoxybenzaldehyde with AlCl₃,²⁸ which was likewise subjected to the dehydration condensation with *o*-phenylenediamine (Scheme 1). The structure and purity of these compounds were fully identified by NMR spectra and elemental analyses. In the ¹H-NMR spectrum of **1** in DMSO-*d*₆, the methoxy proton signal was detected at 4.1 ppm (Fig. S1).³⁰

As judged from the downfield shift of this proton signal compared with those of **2** and **3** at 3.8 ppm (Fig. S2 and S3), the intramolecular hydrogen bonding between amine and ether oxygen was suggested. Namely, a primary O-H...N intramolecular hydrogen bonding likely increases the acidity of imidazole NH proton at the 1-position, which eventually results in the formation of a secondary N-H...O intramolecular hydrogen bonding even in DMSO.



Scheme 1. Synthetic route to **1**.

The single crystal of **1** suitable for the X-ray crystallographic analysis was grown from hexane/ethyl acetate (monoclinic, $P2_1/n$, $Z = 4$). The thermal ellipsoidal model and packing structure are provided in Fig. 2. It was found that the molecules of **1** do not form the face-to-face π - π stacking structure. The torsion angle between hydroxyphenyl and benzimidazole rings is as small as $\theta = 3.1^\circ$, and the distance between O2-H...N2 ($d = 2.53 \text{ \AA}$) is less than the common O-H...N length ($d = 2.80 \text{ \AA}$).

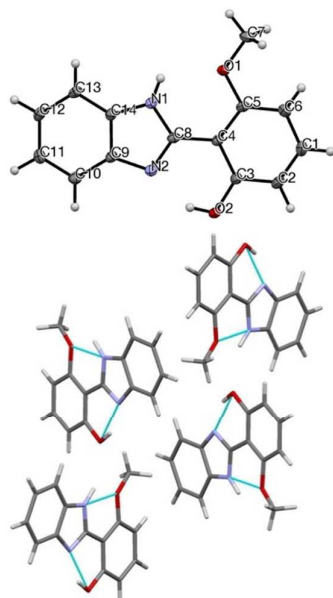


Fig. 2 (Top) Thermal ellipsoidal model of **1**. Ellipsoids are drawn at the 50 % probability level while isotropic hydrogen atoms are represented by spheres of arbitrary size. The labels of hydrogen atoms are omitted for clarity. (Bottom) Packing structure of **1** along the a axis. Light blue lines indicate hydrogen bonding interaction.

In addition, the distance between N1-H...O1 ($d = 2.66 \text{ \AA}$) is less than the common N-H...O length ($d = 2.89 \text{ \AA}$). These results definitely indicate that **1** adopts the nearly coplanar conformation assisted by two kinds of intramolecular hydrogen bonding as discussed above.

At the beginning, the UV-vis absorption emission spectra were measured in THF solution ($10 \mu\text{M}$). Both **1** and **2** showed similar absorption spectra having two relatively sharp peaks below 330 nm, while **3** had a broad peak at around 330nm (Fig. S4). The fluorescence emission spectra excited at the absorption maximum wavelengths are indicated in Fig. 3 and the data are summarized in Table 1. The fluorescence characteristic of **1**, **2**, and **3** are in contrast to that of previously reported **A**. **1** solely emitted a fluorescence at 458 nm. The large Stokes shift (10400 cm^{-1}) and the smooth spectrum feature most probably indicate the ESIPT emission. The fluorescence quantum yield was 0.31. A moderate quantum yield is likely ascribed to the restriction of the C-C bond rotation around phenol and imidazole resulting in the suppression of the transition to the S_1 - T_{ICT} state (*vide supra*).^{19,20} Time-resolved fluorescence spectroscopy measurement using our instrument was impossible due to the short absorption maximum. **2** also exhibited a single emission peak at 450 nm having the Stokes shift of 9300 cm^{-1} . The fluorescence quantum yield (0.17) was smaller than that of **1**. On the other hand, the fluorescence spectrum of **3** consists of two emission bands with the comparable peak intensity. The shorter wavelength emission at 345 nm with the vibronic fine structure is assignable to the locally excited state (LE) emission, while the longer one at 486 nm with the large Stokes shift (12300 cm^{-1}) is originated from the ESIPT emission. The fluorescence quantum yield was considerably low (0.04).

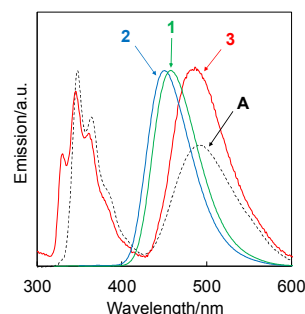


Fig. 3 Fluorescence emission spectra in THF ($10 \mu\text{M}$).

Table 1. Emission characteristics in THF ($10 \mu\text{M}$).

	λ_{em}/nm	Φ^a	LE/ESIPT ^b	Stokes shift ^c / cm^{-1}
1	458	0.31	0/1	10400
2	450	0.17	0/1	9300
3	345, 486	0.04	0.91/1	12300
A	348, 493	<0.01	1.56/1	10200

[a] Calculated based on quinine sulfate as a standard (0.55).

[b] Relative peak intensity of LE and ESIPT emission.

[c] Calculated for ESIPT emission.

ARTICLE

Journal Name

As a consequence, the LE emission was decreased from **A** to **3** and were not observed at all for **1** and **2** indicating that the position of methoxy group has a significant influence on the proton transfer event in the excited state. The ESIPT emission wavelength demonstrated a similar behavior. Namely, the emission maximum of **A** shifted a little to the shorter wavelength for **3**, and exhibited a pronounced blue-shifts for **1** and **2**. This result can be rationalized by the frontier molecular orbital (FMO) theory as Chou et al described.¹⁸ The substitution effect on enol species is expected to be small, while this should be carefully considered for keto species because of the charge transfer from the electron-rich methoxy-substituted phenol ring to the electron-deficient benzimidazole ring. That is, as for the keto species formed in the excited state, the install of electron-donating substituents on the phenol ring results in the destabilization of the highest occupied molecular orbital (HOMO) energy level and brings about the decrease of the energy gap between HOMO and LUMO (the lowest unoccupied molecular orbital). This is likely reflected to the blue-shift of the emission maxima of **1**, **2**, and **3** compared with **A**.

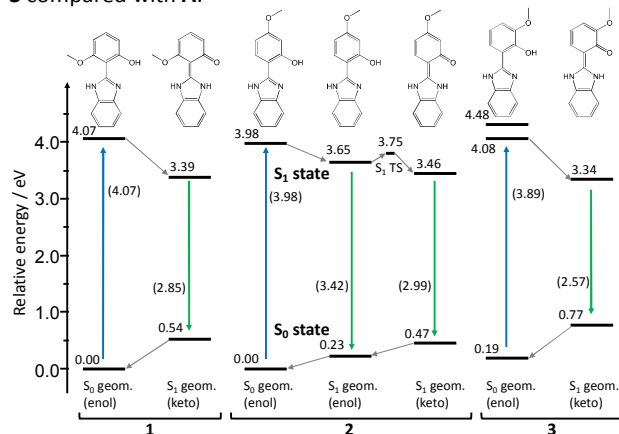


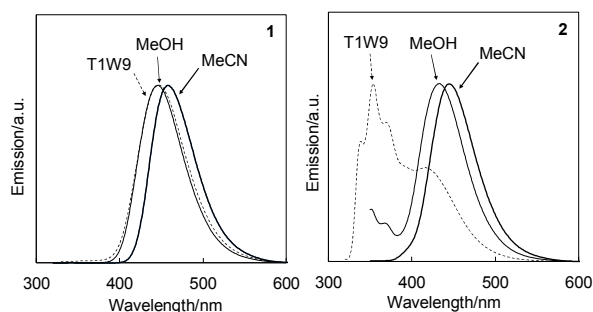
Fig. 4 Energy diagram of **1**, **2**, and **3** in THF calculated by DFT/TDDFT.

Fig. 4 shows the calculated energy diagrams of **1**, **2**, and **3** in THF relative to the S_0 (ground) state of **1**. All the optimized structures were approximately planar. In the S_0 ground state, all molecules favour the enol tautomer as evidenced by the DFT calculation. The oscillator strengths of the S_1 state in the enol form were calculated to be 0.688 and 0.949 for **1** and **2**, respectively, by the TDDFT calculation. Since they were most prominent, the absorption maximum of these molecules can be assigned to the S_0 - S_1 transition. For **3**, the oscillator strength of the S_1 state was 0.346, and that of the S_2 state (excitation energy is 4.29 eV) was calculated to be 0.601. Therefore the absorption maximum of **3** can be assigned to the S_0 - S_2 transition. Subsequently, the excited structures in the S_1 state were deduced from the TDDFT calculation. **1** and **3** takes the keto form only; the enol form was not found as a local minimum. For **2**, the enol form was also found in the S_1 state with the energy barrier of 0.10 eV to the transition state (TS). The fluorescence of **3** was found to exhibit the longer

wavelength in comparison with those of **1** and **2** because the keto form in the S_0 state is relatively unstable for **3**. This feature relates to the HOMO energy level. The HOMO energy levels in the S_1 keto form were -5.33, -5.46, and -5.04 eV, for **1**, **2**, and **3**, respectively, while the LUMO levels of **1**, **2**, and **3** were -1.74, -1.69, and -1.80 eV. The calculated Stokes shifts were 9840, 7985, and 13868 cm^{-1} for **1**, **2**, and **3**, respectively. These computational results qualitatively agree with the experimental findings (Table S5).

Subsequently, the fluorescence emission spectra of three compounds were measured in MeCN and MeOH solutions (10 μM) (Fig. 5, bold and solid lines). Along with the corresponding absorption spectra, the detailed emission characteristics are summarized in Supporting information. As for **1**, the emission maximum was gradually shifted to the shorter wavelength in the order of THF (458 nm), MeCN (456 nm), and MeOH (446 nm). In all cases, no LE emission was observed implying that the double intramolecular hydrogen bonding prompts the smooth proton transfer in the excited state regardless of the solvent character. **2** solely exhibited the ESIPT emission at 444 nm in MeCN, but LE emission at 351 nm was also detected in MeOH. An intramolecular hydrogen bonding of **2** is susceptible to protic solvents and MeOH may interfere the proton transfer in the excited state. On the other hand, the intensities of LE emission and ESIPT emission of **3** were completely reversed by changing from MeCN to MeOH. The ESIPT emission wavelength in MeOH was 462 nm, which unexpectedly showed a bathochromic shift than in MeCN (433 nm). Because the LE emission peak does not have a vibronic fine structure, an interaction of **3** with MeOH is supposed to occur in the excited state (*vide infra*).

We then measured the fluorescence emission spectra in THF/water mixed solvent (10 μM) (Fig. 5, broken line). The compounds were initially dissolved in THF at the concentration of 100 μM , which was diluted with water to adjust as 10 μM . **1** with the robust intramolecular hydrogen bonding solely exhibited the ESIPT fluorescence at 446 nm. The fluorescence spectrum completely overlap with that in MeOH. As can be easily anticipated, the ESIPT emission of **2** was obviously diminished and the LE emission was predominant in THF/water mixed solvent. On the other hand, to our surprise, the fluorescence spectrum of **3** showed an intense ESIPT emission at 431 nm with the Stokes shift of 9800 cm^{-1} in addition to a shoulder LE emission at 354 nm. All three compounds were completely soluble as judged by the zero absorption at 450 nm in the UV-vis absorption spectra (Fig. S5).



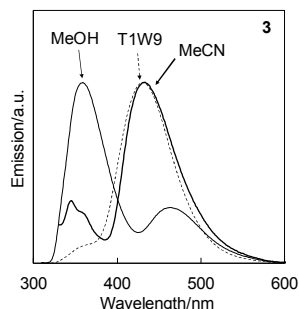


Fig. 5 Fluorescence emission spectra in various solvents (10 μM). Abbreviation T1W9 indicates THF/water mixed solvent in the volume ratio of 1/9.

The calculated emission energetics of **1**, **2**, and **3** in MeOH, MeCN, and H_2O are almost same as that in THF (Table S6). In those polar solvents, only the keto form was obtained in the S_1 state for **1** and **3**. The computational results agree with the observed ES IPT fluorescence of **1**. For **2** both keto and enol forms are found in the S_1 state. In polar solvents, the keto form become unstable, and the barrier height of ES IPT increases (Table S7). Consequently, the LE emission is enhanced in polar solvent. These computational results qualitatively agree with the experimental findings, although the TDDFT calculations seem to underestimate the solvent effects. Our DFT/TDDFT calculations with PCM solvation could not explain the emission behaviors of **3**. We suppose the emission behaviors are attributable to explicit hydrogen-bonds. If we consider several H_2O or MeOH molecules around **3** in the ground state, the molecule becomes nonplanar and the hydrogen atom in OH group tends to take out-of-plane conformation due to hydrogen-bonding with solvents (Fig. S6). This conformation suggests the possibility of solvent-assisted proton transfer in the excited state competing with the direct ES IPT, as well as the abnormal LE emission in polar solvents. The solvent structures and hydrogen-bond networks may be different between in H_2O and MeOH. We guess the strange emission behaviors are attributed to the difference of solvent shell structures in H_2O and MeOH. To verify this hypothesis, we need to study the solvation structures using molecular dynamics simulations; we will continue to investigate this issue.

Finally, the fluorescence emission spectra of three compounds were measured in the crystalline solid state (Fig. 6). The samples used for these measurements were obtained by the recrystallization from, hexane/ethyl acetate, ethanol, and hexane/THF for **1**, **2**, and **3**, respectively. Although **1** showed ES IPT emissions with the fluorescence quantum yield around 0.3 in the solution state irrespective of the solvent character, the fluorescence quantum yield was decreased to 0.16 in the solid state. The emission peak maximum was at 460 nm and no excimer emission at the longer wavelength region was observed. A weak but distinct emission from **1** can be attributed to the absence of π - π stacking interaction (*vide supra*). **2** was almost non-fluorescent in the solid state and the fluorescence quantum yield was 0.01. The dramatic reduction of fluorescence quantum yields is likely stemmed from the

aggregation-caused quenching (ACQ)³¹ due to the electronic interaction between the molecules in the excited state and in the ground state. The single crystal structure of **2** (monoclinic, $P2_1/n$, $Z = 4$) indicates that molecules are arranged in the anti-parallel fashion and form the columnar structure with the close π - π stacking distance of 3.35 Å (Fig. 7). On the other hand, **3** that was weakly emissive in the solution state exhibited a relatively bright fluorescence in the solid state (Fig. 6). The absolute fluorescence quantum yield was 0.26. The emission wavelength at 480 nm was close to that in THF (486 nm) and no LE emission was observed. It is conceivable that an intramolecular hydrogen bonding works more effectively in the solid state which makes the ES IPT process easier. The single crystal structure of **3** (monoclinic, $P2_1/n$, $Z = 4$) indicates the one dimensional hydrogen bonding network (Fig. 7). Namely, not only an intramolecular O-H \cdots N hydrogen bonding but also two kinds of N-H \cdots O intermolecular hydrogen bonding are observed. This intermolecular hydrogen bonding is supposed to accelerate ES IPT resulting in the preferential emission from the keto form.

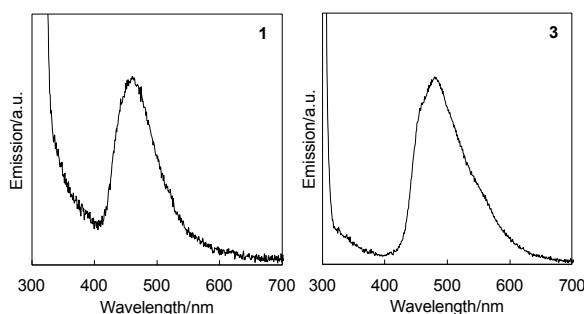


Fig. 6 Fluorescence emission spectra in solid state.

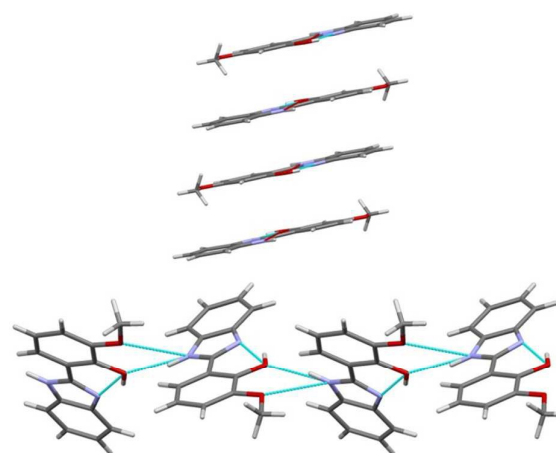


Fig. 7 Packing structure of (top) **2** along the b axis and (bottom) **3** along the a axis. Light blue lines indicate hydrogen bonding interaction.

Conclusions

The ES IPT emission with the large Stokes shift is advantageous for the material application. Although the formation of an

ARTICLE

Journal Name

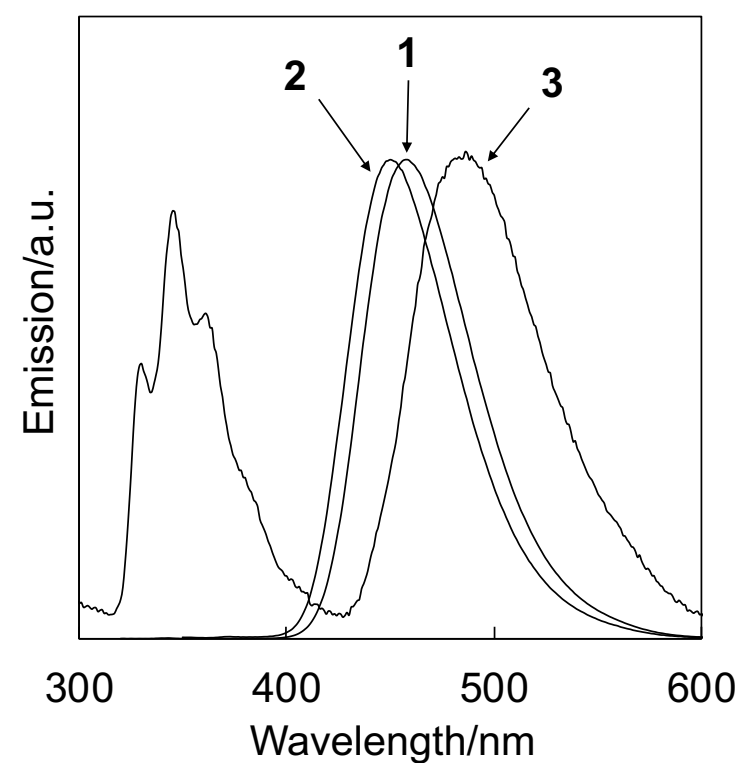
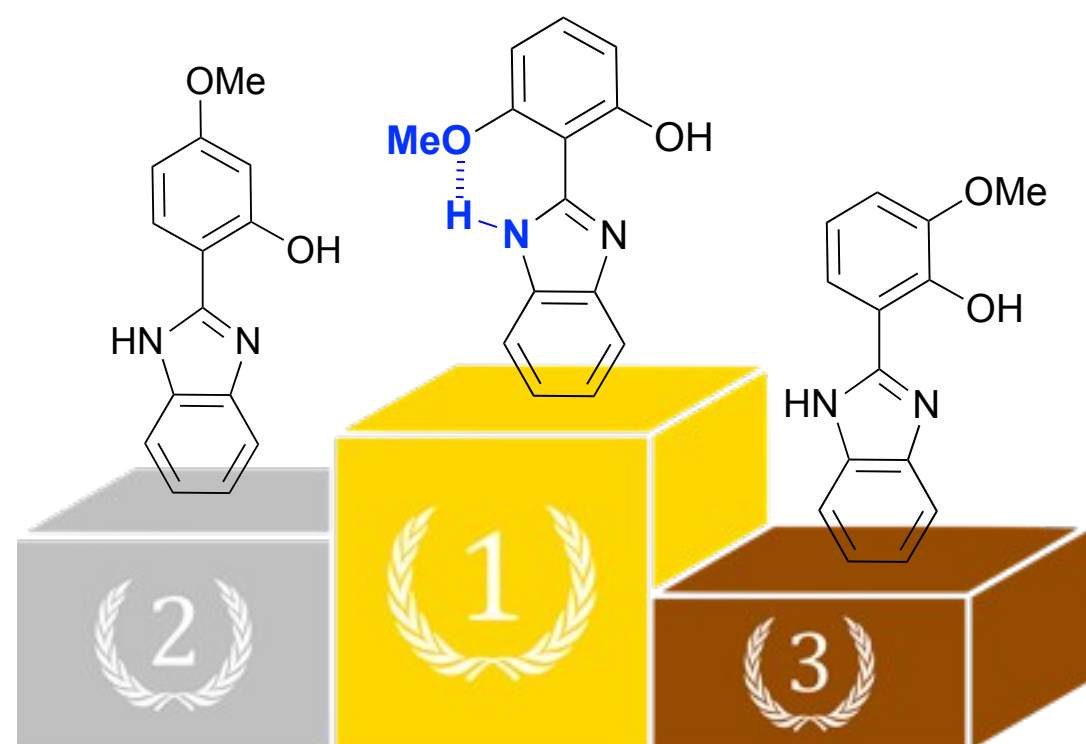
intramolecular hydrogen bonding is preferable for ESIPT, the careful molecular design is required for obtaining an efficient ESIPT. We herein investigated the synthesis and optical characterizations of three 2-hydroxyphenylbenzimidazole isomers having the methoxy group at various positions. In the solution state, the double intramolecular hydrogen bonding was quite effective to realize the robust ESIPT emission. The ratio of LE/ESIPT emissions was influenced by the position of methoxy group. These facts were carefully discussed based on the DFT calculation. In the solid state, the different crystal packing structure such as the columnar π - π stacking and one dimensional hydrogen bonding network resulted in the non-fluorescent and fluorescent behavior, respectively. We believe that the present findings shed light on the design of ESIPT-active π -conjugated molecules.

Acknowledgements

A part of this work was technically supported by the Nanotechnology Platform Program (Molecule and Material Synthesis) of the Ministry of Education Culture, Sports, Science and Technology (MEXT), Japan. A part of this work was financially supported by and performed under the Research Program of "Dynamic Alliance for Open Innovation Bridging Human, Environment and Materials" in "Network Joint Research Center for Materials and Devices". R.F. acknowledges the financial support from a Grant-in-Aid for Scientific Research from Japan Society for the Promotion of Science (JSPS) (26410026). The computations were partially performed at the Research Center for Computational Science, Okazaki, Japan.

Notes and references

- X. Yang, X. Xu, G. Zhou, *J. Mater. Chem. C*, **2015**, *3*, 913–944.
- H. N. Kim, W. X. Ren, J. S. Kim, J. Yoon, *Chem. Soc. Rev.*, **2012**, *41*, 3210–3244.
- B. A. D. Neto, P. H. P. R. Carvalho, J. R. Correa, *Acc. Chem. Res.*, **2015**, *48*, 1560–1569.
- V. S. Padalkar, S. Seki, *Chem. Soc. Rev.*, **2016**, *45*, 169.
- J. Zhao, S. Ji, Y. Chen, H. Guo, P. Yang, *Phys. Chem. Chem. Phys.*, **2012**, *14*, 8803.
- P. K. Sengupta, M. Kasha, *Chem. Phys. Lett.*, **1979**, *68*, 382.
- D. McMorrow, M. Kasha, *J. Phys. Chem.*, **1984**, *88*, 2235.
- S. Park, J. E. Kwon, S. Y. Park, *Phys. Chem. Chem. Phys.*, **2012**, *14*, 8878.
- S. Park, O.-H. Kwon, Y.-S. Lee, D.-J. Jang, S. Y. Park, *J. Phys. Chem. A*, **2007**, *111*, 9649.
- S. Park, J. Seo, S. H. Kim, S. Y. Park, *Adv. Funct. Mater.*, **2008**, *18*, 726.
- S. Park, O.-H. Kwon, S. Kim, S. Park, M.-G. Choi, M. Cha, S. Y. Park, D.-J. Jang, *J. Am. Chem. Soc.*, **2005**, *127*, 10070.
- S. Park, J. E. Kwon, S. H. Kim, J. Seo, K. Chung, S.-Y. Park, D.-J. Jang, B. M. Medina, J. Gierschner, S. Y. Park, *J. Am. Chem. Soc.*, **2009**, *131*, 14043.
- T. Mutai, T. Ohkawa, H. Shono, K. Araki, *J. Mater. Chem. C*, **2016**, *4*, 3599.
- T. Mutai, H. Sawatani, T. Shida, H. Shono, K. Araki, *J. Org. Chem.*, **2013**, *78*, 2482.
- T. Mutai, H. Tomoda, T. Ohkawa, Y. Yabe, K. Araki, *Angew. Chem. Int. Ed.*, **2008**, *47*, 9522.
- Y. Shigemitsu, T. Mutai, H. Houjou, K. Araki, *J. Phys. Chem. A*, **2012**, *116*, 12041.
- K. Skonieczny, A. I. Ciuciu, E. M. Nichols, V. Hugues, M. Blanchard-Desce, L. Flamigni, D. T. Gryko, *J. Mater. Chem.*, **2012**, *22*, 20649.
- A. I. Ciuciu, L. Flamigni, K. Skonieczny, D. T. Gryko, *Phys. Chem. Chem. Phys.*, **2013**, *15*, 16907.
- S. Kim, J. Seo, S. Y. Park, *J. Photochem. Photobiol. A: Chem.*, **2007**, *191*, 19.
- H.-H. G. Tsai, H.-L. S. Sun, C.-J. Tan, *J. Phys. Chem. A*, **2010**, *114*, 4065.
- K.-Y. Chen, C.-C. Hsieh, Y.-M. Cheng, C.-H. Lai, P.-T. Chou, *Chem. Commun.*, **2006**, 4395.
- J. Piechowska, D. T. Gryko, *J. Org. Chem.*, **2011**, *76*, 10220.
- H.-W. Tseng, T.-C. Lin, C.-L. Chen, T.-C. Lin, Y.-A. Chen, J.-Q. Liu, C.-H. Hung, C.-M. Chao, K.-M. Liu, P.-T. Chou, *Chem. Commun.*, **2015**, *51*, 16099.
- D. T. Gryko, J. Piechowska, M. Galezowski, *J. Org. Chem.*, **2010**, *75*, 1297.
- K. Takagi, K. Ito, Y. Yamada, T. Nakashima, R. Fukuda, M. Ehara, D. Takeuchi, *Chem. Lett.*, **2017**, *46*, 1372.
- K. Takagi, K. Ito, Y. Yamada, T. Nakashima, R. Fukuda, M. Ehara, H. Masu, *J. Org. Chem.*, **2017**, *82*, 12173.
- During the course of our investigation, Vullev, Lee, and Gryko and co-workers have reported how to reach intense luminescence for compounds capable of ESIPT using a family of 2-(2'-hydroxyphenyl)benzimidazole derivatives. See, K. Skonieczny, J. Yoo, J. M. Larsen, E. M. Espinoza, M. Barbasiewicz, V. I. Vullev, C.-H. Lee, D. T. Gryko, *Chem. Eur. J.*, **2016**, *22*, 7485.
- D. R. R. Moreno, G. Giorgi, C. O. Salas, R. A. Tapia, *Molecules* **2013**, *18*, 14797.
- P. Ghosh, R. Subba, *Tetrahedron Lett.* **2015**, *56*, 2691.
- The methoxy proton signal of **1** was unchangeably detected at 4.1 ppm in CDCl₃.
- J. B. Birks, *Photophysics of Aromatic Molecules*, Wiley, London, 1970.



A double intramolecular hydrogen bonding enables the efficient ESIPT emission both in solution and solid states.